

Rapid Brightening of 3I/ATLAS Ahead of Perihelion

QICHENG ZHANG ¹ AND KARL BATTAMS ²¹*Lowell Observatory, 1400 West Mars Hill Road, Flagstaff, AZ 86001, USA*²*US Naval Research Laboratory, 4555 Overlook Avenue, SW, Washington, DC 20375, USA*

(Received 2025 October 28)

Submitted to ApJL

ABSTRACT

Interstellar comet 3I/ATLAS has been approaching its 2025 October 29 perihelion while opposite the Sun from Earth, hindering ground-based optical observations over the preceding month. However, this geometry placed the comet within the fields of view of several space-based solar coronagraphs and heliospheric imagers, enabling its continued observation during its final approach toward perihelion. We report photometry from STEREO-A's SECCHI HI1 and COR2, SOHO's LASCO C3, and GOES-19's CCOR-1 instruments in 2025 September–October, which show a rapid rise in the comet's brightness scaling with heliocentric distance r as $r^{-7.5 \pm 1.0}$. CCOR-1 also resolves the comet as an extended source with an apparent coma $\sim 4'$ in diameter. Furthermore, LASCO/CCOR-1 color photometry shows the comet to be distinctly bluer than the Sun, consistent with gas emission contributing a substantial fraction of the visible brightness near perihelion.

Keywords: Interstellar objects (52) — Broadband photometry (184) — Comets (280) — Coronagraphic imaging (313) — Solar instruments (1499)

1. INTRODUCTION

Interstellar comet 3I/ATLAS was discovered on 2025 July 1 at a heliocentric distance $r = 4.5$ au while inbound toward its 2025 October 29 perihelion at $r = 1.36$ au (L. Denneau et al. 2025). At the time, it was comparable in brightness at similar r to the previous interstellar comet, 2I/Borisov (D. Z. Seligman et al. 2025). However, that similarity turned out to be coincidence of timing, as 2I brightened slowly with decreasing heliocentric distance r on its approach, with (observer distance Δ -corrected) brightness scaling as r^{-n} with only $n \approx 2$ —close to that of an inert, reflecting object—over $r \approx 8$ –2 au. Meanwhile, 3I varied in its rate of brightening, but exhibited a much steeper overall $n = 3.8 \pm 0.3$ over $r \approx 6$ –2 au (Q. Ye et al. 2025; J. Tonry et al. 2025; D. Jewitt & J. Luu 2025), perhaps reflecting a difference in nucleus properties or the faster speed at which it approached the Sun.

These photometric observations before and soon after discovery largely measured light scattered by 3I's dust, given the absence of gas emission in near-discovery opti-

cal spectra (e.g., C. Opitom et al. 2025; T. Kareta et al. 2025). However, continued observations from $r = 4$ to 2 au revealed the production of several gaseous species—including OH, CN, Ni I, and Fe I—to have been rising far more steeply, with $n > 8$ (R. Rahatgaonkar et al. 2025; D. Hutsemékers et al. 2025). By 2025 September ($r \sim 2$ au), the comet had developed a green halo enveloping the existing dust coma and tail resembling a typical C₂ gas coma (e.g., images in BAA comet image archive³). Magnitudes reported to the COBS database (J. Zakrajsek & H. Mikuz 2018)⁴ also began deviating sharply above the prior trend, perhaps reflecting the surging gas emission.

Optical observations, however, rapidly became difficult from the ground at $r \lesssim 2$ au as the comet approached its 2025 October 21 superior conjunction at only 1°9 solar elongation from Earth, leaving a gap in this dataset just as the comet approaches its maximum heating at perihelion. However, the comet remained observable during this period to a number of spacecraft around the solar system that are not designed for comet

Corresponding author: Qicheng Zhang
Email: qicheng@cometary.org

³ <https://britastro.org/cometobs/3i>

⁴ <https://cobs.si>

observations, but can nonetheless help to fill in this gap (T. M. Eubanks et al. 2025). Among these spacecraft are several solar observatories with cameras that continually monitor the corona and inner heliosphere, but which also routinely record the passage of comets that happen to cross their fields of view (K. Battams & M. M. Knight 2017). Here, we present observations from solar coronagraphic and heliospheric imagers onboard the STEREO-A, SOHO, and GOES-19 spacecraft, and as well as a cursory analysis of their implications for the 3I’s activity on its final approach toward perihelion.

2. OBSERVATIONS

2.1. Instruments

We present observations of 3I from four cameras onboard three space-based solar observatories, as summarized in Table 1 and detailed below:

1. STEREO (“Solar TERrestrial RELations Observatory”; M. L. Kaiser et al. 2008) is comprised of two effectively identical spacecraft launched in 2006: STEREO-A, which orbits slightly interior to/more quickly than Earth, and STEREO-B, which orbits slightly exterior to/more slowly than Earth. STEREO-B was malfunctioned in and has been defunct since 2014 (D. A. Ossing et al. 2018), so only STEREO-A observed 3I. More specifically, the spacecraft carries a SECCHI (“Sun Earth Connection Coronal and Heliospheric Investigation”; R. A. Howard et al. 2008) instrument suite, of which we report observations from two cameras:

- (a) HI1 (“Heliospheric Imager 1”; C. Eyles et al. 2009) observes a $20^\circ \times 20^\circ$ field at a normally 2×2 -binned scale of $72 \text{ arcsec px}^{-1}$, centered 14° from the Sun along the Sun–Earth line. The camera observes through a filter with a pre-flight full-width half-maximum (FWHM) wavelength span of $\sim 615\text{--}740 \text{ nm}$, as well as a blue leak near 400 nm and a red leak near 1000 nm (D. Bewsher et al. 2010), with later testing with a flight spare suggesting that the bandpass may have shifted blueward by $15\text{--}20 \text{ nm}$ (J.-P. Halain 2012). STEREO-A HI1 observed 3I over 2025 September 11–27.
- (b) COR2 (“CORonagraph 2”) covers $\sim 0.7\text{--}4^\circ$ elongation at $15 \text{ arcsec px}^{-1}$ through a $\sim 670\text{--}750 \text{ nm}$ bandpass filter as well as a rotating polarizer. It collects two types of images: polarized sequences of three images with the polarizer rotated 0° , 120° , and 240° , and non-polarized images made from a sum of consecutive exposures with the polarizer at 0° and

90° . Most of the data is of the latter variety, and we only present results from these unpolarized data. STEREO-A COR2 observed 3I over 2025 September 28–October 2. Note that the comet’s superior conjunction from STEREO-A was on September 30—well before the October 21 conjunction from Earth—due to STEREO-A orbiting $\sim 47^\circ$ ahead of Earth during this time.

2. SOHO (“Solar and Heliospheric Observatory”; V. Domingo et al. 1995), launched 1995, orbits the Sun–Earth L1 point, carrying the LASCO (“Large Angle and Spectrometric CORonagraph”; G. Brueckner et al. 1995) coronagraphs. Its wide field coronagraph, C3, covers $\sim 1^\circ\text{--}8^\circ$ elongation at $56 \text{ arcsec px}^{-1}$ primarily through its $\sim 520\text{--}770 \text{ nm}$ Clear filter, although it also has an assortment of less frequently used color filters. LASCO C3 observed 3I over 2025 October 15–26, shortly before the comet’s October 29 perihelion.
3. GOES-19 was launched in 2024, and is primarily a weather satellite operating in a geostationary orbit. However, it also carries the CCOR-1 (“Compact CORonagraph 1”; A. Thernisien et al. 2025) coronagraph for operational space weather monitoring. CCOR-1 covers $\sim 1^\circ\text{--}6^\circ$ elongation at $19 \text{ arcsec px}^{-1}$ with a $\sim 470\text{--}740 \text{ nm}$ bandpass, and observed 3I concurrently with LASCO C3 over 2025 October 18–24.

All observations of 3I by these instruments were made as part of their standard observing routine.

2.2. Data

We processed images from all instruments similarly following a procedure similar to that used by Q. Zhang et al. (2023), and started from the level-2 HI1, level-0 COR2, level-0.5 C3 (plus level-1 vignetting/bias correction), and level-1b CCOR-1 data. We first derived astrometric solutions for all coronagraph (COR2, C3, and CCOR-1) frames using Gaia DR3 (Gaia Collaboration et al. 2023), but used the existing HI1 solutions. We subtracted a stray light/corona model from all coronagraph frames, derived from an average of all frames in each dataset; level-2 HI1 data already includes this correction. We also subtracted a stellar background from each HI1 frame, derived from frames several hours away to avoid self-subtraction of the moving comet.

For all frames, we extracted cutouts centered on the ephemeris position (JPL orbit #27) and stacked these comet-centered cutout frames. Stacking was critical to

Table 1. Summary of observations of 3I/ATLAS

Spacecraft	Instrument	Bandpass (nm) ^a	Observation Dates ^b	r (au) ^c	Δ (au) ^d	α (°) ^e	ε (°) ^f
STEREO-A	SECCHI HI1	595–720	2025 Sep 11–26	1.79–2.20	2.75–3.04	2.7–10.4	5.0–24.3
	SECCHI COR2	670–750	2025 Sep 28–Oct 2	1.68–1.77	2.64–2.73	1.7–2.4	3.1–4.2
SOHO	LASCO C3	520–770 ^g	2025 Oct 15–26	1.36–1.45	2.33–2.42	1.8–5.9	2.6–8.4
GOES-19	CCOR-1	470–740	2025 Oct 18–24	1.37–1.42	2.35–2.41	1.9–3.7	2.6–5.3

^aFWHM wavelength range (J.-P. Halain 2012; G. H. Jones et al. 2018; A. Thernisien et al. 2025).

^bDates on which the comet was within the instrument field of view, even if unobservable due to interference from stray light, background objects, coronal structure, etc.

^cComet heliocentric distance.

^dObserver–comet distance.

^ePhase angle.

^fSolar elongation.

^gFor the primary, Clear filter; measured from published transmission + quantum efficiency curves.

our analysis to smooth out background features and single frame image defects (e.g., stars, coronal structure, cosmic rays/solar energetic particles, etc.) and to obtain images with sufficiently high S/N for analysis. In fact, only in CCOR-1 data is 3I only clearly visible in individual frames; in HI1, the comet can be marginally seen in a subset of frames at the noise level, while in COR2 and C3, the comet cannot be seen at all without stacking. No offset in the comet’s observed position could be distinguished from the ephemeris position at the resolution of any of the data, so we applied no further corrections to the ephemeris position.

Figure 1 shows the stack on the comet through each of the four instruments. The CCOR-1 stack resolves the comet as extended with a $\sim 4'$ diameter coma, compared to a similarly stacked star nearby that serves as an approximate point spread function (PSF). No tail is clearly visible, although the duration of the stack combined with the low ($<4^\circ$) phase angle means that an ion tail—which could vary in direction with the solar wind $\sim 10^\circ$ from the radial direction (Y. R. Fernández et al. 1997)—could theoretically point in any projected direction on the individual frames, so may simply be smeared out, perhaps contributing to the apparent coma. Any physically antisunward dust tail would also be highly foreshortened by this geometry. Note also that the sunward direction rotated by 125° over the time range of the stack, so any angularly sunward-aligned structures would likewise be smeared out; however, the sunward-aligned stack does not appear qualitatively different from the presented north-aligned stack, so is not shown.

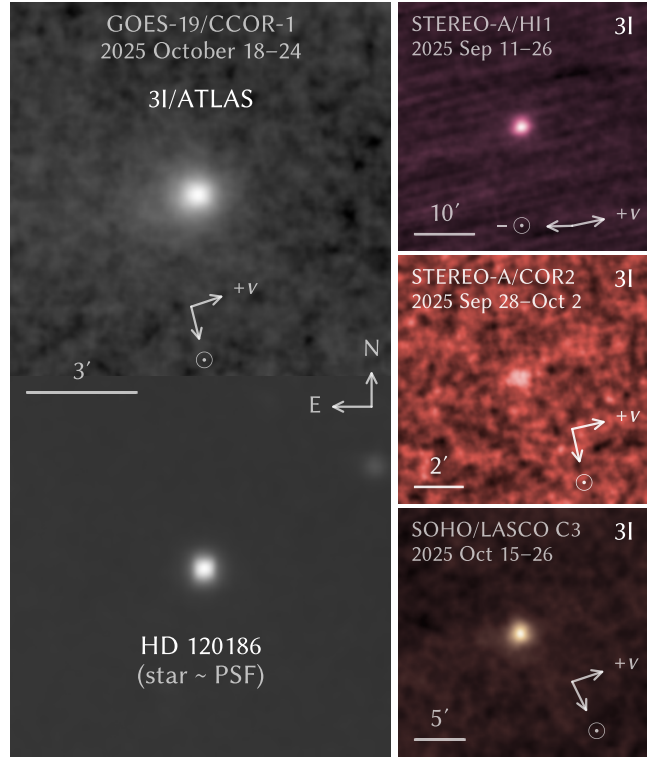


Figure 1. Left: Stack of all CCOR-1 frames of 3I/ATLAS (top), and an equivalent stack centered on a nearby star on the same frames, approximating the PSF (bottom). Right: Similar stacks of all HI1 (top), COR2 (middle), and LASCO C3 Clear (bottom) frames of 3I. All stacks are aligned with north up. The heliocentric velocity ($+v$), and sunward (\odot) or antisunward (\ominus) directions are labeled for the comet at the midpoint time.

For time series photometry, we stacked the cutouts over over 1 day windows, except for COR2 where we split the data into a pair of 2.5 day/1.7 day stacks with similar S/N, due to the low total S/N of that dataset being insufficient for useful 1 day stacks. We measured the flux within radii of $3'$ for HI1, $1'$ for COR2, and $2.5'$ for both C3 and CCOR-1—which we estimate capture $\gtrsim 90\%$ of the comet’s flux visible above the noise level in the full image stack for each dataset—and converted them to the conventional solar magnitude system (i.e., Sun as -26.76 at $r = 1$ au, its Johnson V magnitude; C. N. Willmer 2018), which is convenient for distinguishing differences from solar color. We used the existing photometric calibrations of S. Tappin et al. (2022) for HI1 and Q. Zhang et al. (2023) for C3. For COR2 and CCOR-1, we followed the same procedure Q. Zhang et al. (2023) used for LASCO, and derived zero-point magnitudes of 12.5 and 14.7 from 2025 April and May observations of the Sun-like star 39 Tau, respectively.

Figure 2 presents all of the resulting photometry that detected the comet at $> 3\sigma$, corrected to a common $\Delta = 1$ au. No phase corrections were applied, as the data cover a narrow phase angle range $\alpha = 1.7^\circ\text{--}10.4^\circ$, and the necessary dust-to-gas brightness ratio such a correction would depend on is unknown. Note, however, that any direct photometric fit across all points would implicitly assume the comet is solar-colored between the relevant instrument bandpasses, which is not necessarily true, as demonstrated by the offset between the contemporaneous CCOR-1 and LASCO C3 Clear photometry. While all four bandpasses have similar effective wavelengths of $\sim 600\text{--}700$ nm, the variations in their spectral profiles still produce differences in sensitivity to common optical gas species, particularly CN, C_2 , and NH_2 (Q.-Z. Ye et al. 2014; G. H. Jones et al. 2018).

LASCO actually has the capability to directly measure color: while it takes the vast majority of its data through its Clear filter (including the data used for the time series photometry in Figure 2), it also presently takes one full resolution frame per day through each of its Blue, Orange, DeepRd (“deep red”), and IR (infrared) color filters, whose properties are detailed in G. Brueckner et al. (1995) and A. Thernisien et al. (2006). Stacking all the frames through each color filter yields detections of 3I in only the Blue and Orange stacks, in which the comet was respectively (-0.7 ± 0.2) mag and (-0.4 ± 0.2) mag brighter than in the equivalent Clear-filtered stack—distinctly bluer than solar color, in contrast to the comet’s red dust (C. Opitom et al. 2025; T. Kareta et al. 2025). The Blue bandpass efficiently transmits the C_2 Swan bands, while the Orange bandpass is

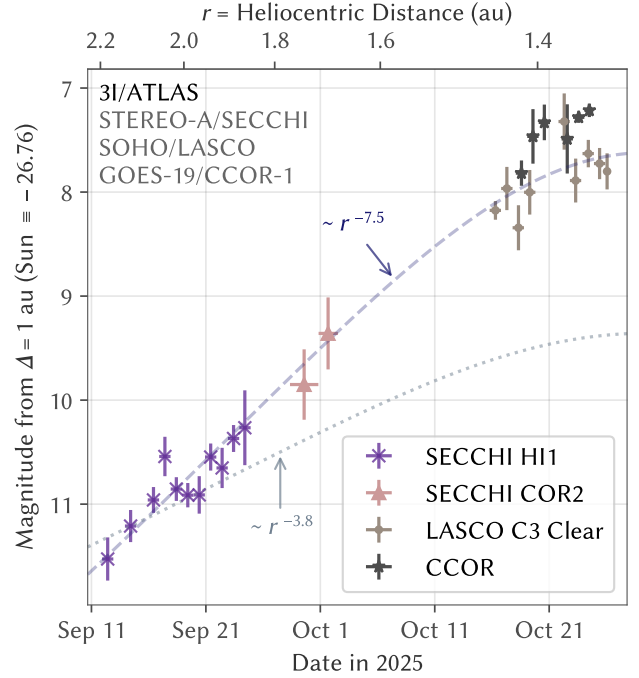


Figure 2. Light curve of daily (and COR2 2.5 day/1.7 day) photometry, corrected to $\Delta = 1$ au, along with the $r^{-7.5}$ best fit brightness scaling (for which the CCOR-1 points incorporate a $+0.4$ mag color correction to match the C3 Clear flux) and an $r^{-3.8}$ curve matching the previously reported trend at $r \gtrsim 2$ au with an arbitrary vertical placement. Note also that the magnitude error bars indicate only the flux measurement uncertainty (i.e., the noise in the S/N of each detection) and do not include the estimated $\lesssim 0.1$ mag uncertainties in the photometric calibrations.

less sensitive to C_2 but efficiently transmits several NH_2 bands (H. Kawakita & J.-i. Watanabe 2002; G. H. Jones et al. 2018), suggesting that the presence of these species could be at least partly responsible for the observed deviations from solar colors. The LASCO C3 photometry can also be compared with the contemporaneous CCOR-1 photometry, which are measured with the same photometric aperture size. CCOR-1’s bandpass is similar to, but ~ 40 nm bluer than, the C3 Clear bandpass, increasing CCOR-1’s relative sensitivity to the C_2 Swan bands. Indeed, the comet’s CCOR-1 brightness falls between the C3 Blue and Clear values, with a CCOR-1–Clear color of (-0.4 ± 0.1) mag. Table 2 provides the observed (i.e., not Δ -corrected) magnitudes through each filter.

Unlike C3 Clear and CCOR-1, neither HI1 nor COR2 are sensitive to the C_2 Swan bands. However, both instruments have much narrower primary bandpasses covering multiple NH_2 bands, offsetting the lack of C_2 sensitivity with increased NH_2 sensitivity. While these NH_2 bands are normally much fainter than the C_2 Swan

Table 2. LASCO C3 + CCOR-1 color photometry

Filter	Bandpass (nm) ^a	Observed Magnitude ^b
C3 Clear	520–770	9.82 ± 0.07
C3 Blue	440–520	9.13 ± 0.20
C3 Orange	550–630	9.42 ± 0.14
C3 DeepRd	720–800	>9.3 (3σ)
C3 IR	840–900	>9.3 (3σ)
CCOR-1	470–740	9.40 ± 0.08

^aFWHM wavelength range; computed for LASCO C3 from published filter transmission + quantum efficiency curves; CCOR-1 values from A. Thernisien et al. (2025).

^bComet magnitude measured from a stack of all frames through each filter. Note that the stated uncertainties do not include the estimated $\lesssim 0.1$ mag uncertainties in the photometric calibrations.

bands (A. L. Cochran et al. 2015), 3I has been found to be C₂-depleted (D. Hutsemékers et al. 2025), which may improve the trade balance if C₂ is still depleted. HI1’s red and blue leaks also provide sensitivity to CN, while it remains unknown if COR2 has similar leaks. A rigorous quantitative analysis requires an accurate inventory of the comet’s optical emission and dust brightness, neither of which is available.

For our cursory analysis, we consider that the comet’s brightness in HI1 and COR2 would likely more similar to that in C3 Clear than in CCOR-1, and “correct” the CCOR-1 photometry to match the equivalent C3 Clear brightness (i.e., by applying a +0.4 mag offset) for the global fit. We then also allow for the possibility that HI1/COR2 brightness is offset from C3 Clear by a similar ~ 0.4 mag. With these color corrections, we obtain $n = 7.5 \pm 1.0$ (with a corresponding normalized magnitude $M_1 = 5.1 \pm 0.2$ at $r = 1$ au)—much steeper than the $n = 3.8 \pm 0.3$ previously reported for the comet’s earlier brightening trend at $r \gtrsim 2$ au (D. Jewitt & J. Luu 2025).

Note that the standard Johnson *V* bandpass is far more sensitive to C₂ and NH₂ than the C3 Clear bandpass due to the former covering a much narrower range isolating this emission, like C3 Blue or Orange. Consequently, we expect the C3 Blue or Orange brightness— ~ 0.4 – 0.7 mag above the fitted curve—to better represent the true *V* brightness of the comet.

3. DISCUSSION

While ground-based optical observations have been hindered by the comet’s low solar elongation over much

of our observation period, radio observations are less adversely impacted by this geometry, and J. Crovisier et al. (2025) recently reported a detection of OH radio emission over October 13–19 ($r = 1.4$ au) corresponding to a production rate of $(5.7 \pm 0.6) \times 10^{28}$ molecules s^{−1}. For comparison, the last pre-conjunction optical OH measurement by D. Hutsemékers et al. (2025) on September 12 ($r = 2.19$ au) yielded a production rate of $10^{27.15 \pm 0.10}$ molecules s^{−1}. The power curve linking these two production rate measurements of OH—often used as a proxy for H₂O, which is typically the primary source of OH for comets—has $n = 8.3 \pm 0.6$, which is quite similar to the $n = 7.5 \pm 1.0$ we obtained for the comet’s optical brightness.

Note that these two n are not necessarily directly comparable as the optical brightness of a comet does not scale with its H₂O or overall gas production unless all of the following conditions are met:

1. The observed optical brightness is predominantly from gas emission and not dust, whose brightness involves a further r^{-2} term corresponding to the variation of intercepted sunlight, as well as complications related to the dust’s residence time in the photometric aperture.
2. The aperture encompasses all of the emission from the gas from formation/release through photodissociation or ionization, in which case, measured brightness has a r^2 scaling from gas lifetime that exactly offsets the r^{-2} scaling of fluorescence efficiency.
3. The Swings effect (P. Swings 1941)—variations in the fluorescence efficiency with heliocentric radial velocity—is negligible.
4. The mixing ratios of the optical gases is constant over the observation period, so the production rates of these gases scale with the H₂O or overall gas production rate.

Condition 1 is plausible given the comet’s lack of a prominent dust tail and blue color, but significant dust contribution to the brightness cannot be ruled out with just the presented data—particularly for HI1 and COR2, which are insensitive to C₂. NH₂ is the major gas species that HI1 and C3 Clear (and CCOR-1, corrected to C3 Clear)—which anchor the two ends of the fit—are both sensitive to. Condition 2 is satisfied for NH₂, as scale length for destruction (U. Fink et al. 1991) is contained within all the aperture radii we used, apart from the low S/N COR2 photometry that negligibly contributes to the fit. The Swings effect is usually neglected for NH₂

when deriving their production rates (A. L. Cochran et al. 2015), satisfying condition 3. The status of condition 4 is not directly known, although the closeness of the n in the comparison above and the possible satisfaction of the other three conditions hints at its possible validity.

Following its 2025 October 29 perihelion, 3I makes a return to twilight and subsequently dark, night skies over 2025 November–December. Ground-based observations will then, once again, be able to characterize the comet in far greater detail than possible with the data we have presented, whose value lies primarily in bridging the gap in ground-based optical observations during a critical period in the comet’s evolution. Our cursory analysis of this data indicates the comet will likely emerge from conjunction considerably brighter than when it entered, with an extrapolated geocentric V magnitude of ~ 9 at perihelion, perhaps driven by prominent, visible gas emission.

The reason for 3I’s rapid brightening, which far exceeds the brightening rate of most Oort cloud comets at similar r (C. E. Holt et al. 2024), remains unclear. It is possible that its H_2O sublimation had been held down earlier by cooling from its CO_2 sublimation, which remained unusually dominant at $r \sim 3$ au (C. Lisse et al. 2025; M. A. Cordiner et al. 2025), perhaps related to its rapid approach toward the Sun compared to other comets. Oddities in nucleus properties like composition, shape, or structure—which might have been acquired from its host system or over its long interstellar journey—may likewise contribute. Without an established physical explanation, the outlook for 3I’s post-perihelion behavior remains uncertain, and a plateau in brightness—or even a brief continuation of its pre-perihelion brightening—appears as plausible as rapid fading past perihelion. Continued observations may help provide a more definitive explanation for the comet’s behavior.

4. CONCLUSIONS

We presented observations of interstellar comet 3I/ATLAS in solar coronagraphic and heliospheric imagery from the STEREO/SECCHI, SOHO/LASCO, and GOES-19/CCOR-1 instruments as the comet approached perihelion while near superior conjunction

from Earth. We performed image stacking and photometry with these data, and obtained the following results:

1. The comet appears extended in a stack of all CCOR-1 frames of the comet, with an apparent $\sim 4'$ diameter coma.
2. The comet rapidly brightened on its final approach toward perihelion over 2025 September–October at heliocentric distances of $r \lesssim 2$ au, with a much steeper r^{-n} brightness scaling of $n = 7.5 \pm 1.0$ than the $n = 3.8 \pm 0.3$ previously reported at $r \gtrsim 2$ au. The trend extrapolates to a geocentric V magnitude of ~ 9 at perihelion.
3. The comet appears distinctly bluer than the Sun in LASCO/CCOR-1 color photometry—in contrast to earlier observations showing the comet’s dust to be red—suggesting that gas emission, likely from C_2 and possibly NH_2 , contributes a sizable fraction of the overall visible brightness.

ACKNOWLEDGMENTS

Q.Z. was supported as a Percival Lowell Postdoctoral Fellow at Lowell Observatory. K.B. was supported by the NASA-funded Sungrazer project.

The STEREO/SECCHI data are produced by an international consortium of the NRL, LMSAL, NASA GSFC (USA), RAL and the University of Birmingham (UK), MPS (Germany), CSL (Belgium), and IOTA and IAS (France). The SOHO/LASCO data are produced by a consortium of the NRL (USA), MPS (Germany), Laboratoire d’Astronomie (France), and the University of Birmingham (UK). SOHO is a project of international cooperation between ESA and NASA.

Facilities: GOES (CCOR-1), SOHO (LASCO), STEREO (SECCHI)

Software: Astropy (Astropy Collaboration et al. 2013, 2018, 2022), Astroquery (A. Ginsburg et al. 2019), Matplotlib (J. D. Hunter 2007), NumPy (S. Van Der Walt et al. 2011; C. R. Harris et al. 2020), SciPy (P. Virtanen et al. 2020)

REFERENCES

- Astropy Collaboration, Robitaille, T. P., Tollerud, E. J., et al. 2013, *A&A*, 558, A33
- Astropy Collaboration, Price-Whelan, A. M., Sipőcz, B., et al. 2018, *AJ*, 156, 123
- Astropy Collaboration, Price-Whelan, A. M., Lim, P. L., et al. 2022, *ApJ*, 935, 167
- Battams, K., & Knight, M. M. 2017, *RSPTA*, 375, 20160257

- Bewsher, D., Brown, D., Eyles, C., et al. 2010, *SoPh*, 264, 433
- Brueckner, G., Howard, R., Koomen, M., et al. 1995, *SoPh*, 162, 357
- Cochran, A. L., Levasseur-Regourd, A.-C., Cordiner, M., et al. 2015, *SSRv*, 197, 9
- Cordiner, M. A., Roth, N. X., Kelley, M. S., et al. 2025, *ApJL*, 991, L43
- Crovisier, J., Biver, N., & Bockelee-Morvan, D. 2025, *CBET*, 5625
- Denneau, L., Siverd, R., Tonry, J., et al. 2025, *MPEC*, 2025-N12
- Domingo, V., Fleck, B., & Poland, A. I. 1995, *SoPh*, 162, 1
- Eubanks, T. M., Bills, B. G., Hibberd, A., et al. 2025, *arXiv:2508.15768*
- Eyles, C., Harrison, R., Davis, C. J., et al. 2009, *SoPh*, 254, 387
- Fernández, Y. R., McFadden, L. A., Lisse, C. M., Helin, E. F., & Chamberlin, A. B. 1997, *Icar*, 128, 114
- Fink, U., Combi, M. R., & Disanti, M. A. 1991, *ApJ*, 383, 356
- Gaia Collaboration, Vallenari, A., Brown, A. G., et al. 2023, *A&A*, 674, A1
- Ginsburg, A., Sipőcz, B. M., Brasseur, C., et al. 2019, *AJ*, 157, 98
- Halain, J.-P. 2012, PhD thesis, Université de Liège
- Harris, C. R., Millman, K. J., Van Der Walt, S. J., et al. 2020, *Natur*, 585, 357
- Holt, C. E., Knight, M. M., Kelley, M. S., et al. 2024, *The Planetary Science Journal*, 5, 273
- Howard, R. A., Moses, J., Vourlidas, A., et al. 2008, *SSRv*, 136, 67
- Hunter, J. D. 2007, *CSE*, 9, 90
- Hutsemékers, D., Manfroid, J., Jehin, E., et al. 2025, *arXiv:2509.26053*
- Jewitt, D., & Luu, J. 2025, *arXiv:2510.18769*
- Jones, G. H., Knight, M. M., Battams, K., et al. 2018, *SSRv*, 214, 20
- Kaiser, M. L., Kucera, T., Davila, J., et al. 2008, *SSRv*, 136, 5
- Kareta, T., Champagne, C., McClure, L., et al. 2025, *ApJL*, 990, L65
- Kawakita, H., & Watanabe, J.-i. 2002, *ApJ*, 572, L177
- Lisse, C., Bach, Y., Bryan, S., et al. 2025, *RNAAS*, 9, 242
- Opitom, C., Snodgrass, C., Jehin, E., et al. 2025, *MNRAS*, 544, L31
- Ossing, D. A., Cox, M. W., Wilson, D., et al. 2018, in *SpaceOps Conference*, Vol. 2018, 2565
- Rahatgaonkar, R., Carvajal, J. P., Puzia, T. H., et al. 2025, *arXiv:2508.18382*
- Seligman, D. Z., Micheli, M., Farnocchia, D., et al. 2025, *ApJL*, 989, L36
- Swings, P. 1941, *LicOb*, 19, 131
- Tappin, S., Eyles, C., & Davies, J. 2022, *SoPh*, 297, 37
- Thernisien, A., Morrill, J., Howard, R., & Wang, D. 2006, *SoPh*, 233, 155
- Thernisien, A., Chua, D., Carter, M., et al. 2025, *arXiv:2508.13467*
- Tonry, J., Denneau, L., Alarcon, M., et al. 2025, *arXiv:2509.05562*
- Van Der Walt, S., Colbert, S. C., & Varoquaux, G. 2011, *CSE*, 13, 22
- Virtanen, P., Gommers, R., Oliphant, T. E., et al. 2020, *NatMe*, 17, 261
- Willmer, C. N. 2018, *ApJS*, 236, 47
- Ye, Q., Kelley, M. S., Hsieh, H. H., et al. 2025, *arXiv:2509.08792*
- Ye, Q.-Z., Hui, M.-T., Kracht, R., & Wiegert, P. A. 2014, *ApJ*, 796, 83
- Zakrajsek, J., & Mikuz, H. 2018, *JBAA*, 128
- Zhang, Q., Battams, K., Ye, Q., Knight, M. M., & Schmidt, C. A. 2023, *PSJ*, 4, 70